PAPER

Check for updates

A plasmonic AuPd bimetallic nanoalloy decorated over a GO/LDH hybrid nanocomposite *via* a green synthesis route for robust Suzuki coupling reactions: a paradigm shift towards a sustainable future

Mitarani Sahoo,[a] Sriram Mansingh,[a] Satyabrata Subudhi, [iD][a] Priyabrat Mohapatra[b] and Kulamani Parida [iD]*[a]

Exploiting the advantageous science of layered architectures, herein graphene oxide (GO) and a ZnCr-layered double hydroxide (LDH) have been united together and further modified by Au–Pd noble metal nanoparticles (NPs) to design a highly efficient novel GO/LDH@AuPd hybrid photocatalyst. The synthesis of this hybrid composite was carried out *via* the *in situ* nucleation of the ZnCr LDH over the surface of GO sheets, subsequently followed by the photo-deposition of bimetallic alloyed NPs and the reduction of graphene oxide (GO) to reduced graphene oxide (RGO) under light illumination. The successful formation of a GO/LDH@AuPd hybrid material was evidenced *via* XRD, UV-vis spectroscopy, TEM and XPS analysis. Here XPS techniques were employed to assess the electronic contribution of LDH towards the electron density on the noble metal through the GO surface during the photoreduction process. TEM images confirmed that bimetallic NPs are well dispersed on the LDH as well as over the GO surface. Moreover, the significant quenching of the PL intensity and the smaller arc radius of EIS measurements of an active AuPd alloyed sample demonstrate effective charge separation leading to superb photocatalytic activity. Here, an energy saving and green synthesis method was adopted by utilizing (i) visible-light active Zn–Cr-LDH nanoplates, (ii) SPR-effective gold NPs, (iii) the channelling features of GO, (iv) the charge heterogeneity of the AuPd alloy and (v) the efficiency of palladium towards the C–C coupling reaction, which made the catalyst more powerful in terms of enhancing the photocatalytic Suzuki coupling reaction compared to various chemical agents at high temperatures. The existence of Au enhances the abilities of Pd synergistically together with GO/LDH in the presence of visible light, boosting Suzuki coupling reactions. The Suzuki coupling product yield, *i.e.*, biphenyl, is around 99.5% over the GO/LDH@AuPd composite, which is about 1.9 times higher than a single metal loaded GO/LDH composite. The enhanced catalytic activity resulted from the electron transfer pathways of LDH → Au → Pd and LDH → RGO → Au → Pd in the hybrid nano-architecture. We believe that this novel approach can lead to stable heterogeneous photocatalysts for other reactions with high activities.

Introduction

The scarcities of fossil fuels and the ecological effects of their emissions have become major hurdles in the race for social progress. The use of solar energy to trigger organic reactions has achieved enormous attention owing to the resulting sustainable and greener reaction conditions. Considering this, recently, ZnCr layered double hydroxides (LDHs) have appeared as a ground-breaking photocatalyst in the context of energy and environmental applications owing to their enhanced photocatalytic activity.[1] However, naked LDHs typically acquire low quantum yields under visible light irradiation because of worse electron–hole transfer properties and poor charge carrier mobility.[2] Therefore, a lot of attempts have been made to further enhance the photocatalytic activities of LDHs through the inclusion of 2D-layered carbon materials like graphene oxide (GO).[3] Graphene (and its derivatives GO and RGO) has become a rising star in the field of catalysis owing to its good anchoring sites for semiconductor/

[a] *Centre for Nano Science and Nano Technology, Siksha 'O' Anusandhan (Deemed to be University), Bhubaneswar-751 030, Odisha, India. E-mail: paridakulamani@yahoo.com, kulamaniparida@soauniversity.ac.in; Fax: +91 674 2350642; Tel: +91 674 2351777*
[b] *Department of Chemistry, C.V.Raman College of Engineering, Bidyanagar, Mahura, Janla, Bhubaneswar-752 054, Odisha, India*

metal nanoparticles (NPs) and because of its excellent conductivity, charge separation abilities, and high chemical and mechanical stabilities.[4,5] Furthermore, a GO/LDH composite supporting bimetallic NPs not only enhances the photocatalytic properties of the alloyed NPs, but it also induces synergistic effects caused by the tremendous conductivity and high surface area of the graphene nanosheets. For greater improvement of the photocatalytic activity and stability, Au, with its plasmonic properties, can be blended with Pd to form a AuPd alloy, which can make full use of solar photons in the visible spectral region. More importantly the individual moieties not only retain their own properties but, at the same time, they generate new features when placed together within close proximity. As a result, hybrid nanomaterials provide an exciting platform to study the combined effects of Au and Pd for photocatalytic organic conversion.

In the present research era, bimetallic NPs have stolen the limelight when it comes to the photocatalytic synthesis of organic compounds. Furthermore, bimetallic AuPd alloyed NPs have been synthesized on various semiconducting supports, like TiO_2[6] and $BiVO_4$,[7] and also on electronic conductors like graphene[8–10] to enhance the catalytic efficiency. On the other hand, the synthesis of bimetallic NPs with properly controlled morphologies and compositions over semiconducting materials, like layered double hydroxides, has been effectively used to restrict the nanosize effect shown by alloyed NPs during photocatalysis. Recently, AuPd/MgAl-LDH was reported to exhibit excellent photocatalytic performance for the selective oxidation of benzyl alcohol to benzaldehyde.[11] Although bimetallic NPs supported over GO or LDH individually have been studied enormously, photoreduction with bimetallic AuPd supported over a GO/LDH hybrid nanocomposite has been reported rarely. To the best of the authors' knowledge, no article to date has explored the photocatalytic potential, along with the structural importance, of GO/LDH@AuPd ternary nanohybrids towards organic synthesis. So, the development of this proficient photocatalyst, which can acquire huge benefit from the active groups, encourage the charge transfer efficiency of photo-induced charge carriers, and be utilized properly in a single reaction system, is still a burning topic research.

Moreover, particular focus is needed on the simultaneous utilization of photo-generated holes and electrons for organic reactions, which can provide a promising catalytic pathway for eco-friendly and economical synthesis. Recently many reports have mainly focused on the utilization of photo-generated electrons and holes for reduction and oxidation reactions, respectively,[12,13] but coupling reactions have remained relatively untouched with regards to the utilization of light. In the present era of organic research, coupling reactions conducted using visible-light active materials can be found on the cover pages of many scientific reports. However, few literature reports cover visible-light active materials for photocatalytic Suzuki coupling reactions,[14–16] as major photocatalysts suffer from (i) low light absorption capacities, (ii) poor photostabilities and (iii) faster charge recombination

properties. Recently, Sun et al. reported Suzuki coupling reactions over various MOF-based photocatalysts (i.e., metal@MOFs) under visible light irradiation.[17,18] Additionally, light-driven photocatalysts have materialized as one of the cleanest, most cost effective and environmentally friendly techniques for the elimination of environmental toxic waste and alleviating the energy crisis. For that reason, the scientific community has devoted its abilities and knowledge towards the fabrication of highly efficient visible-light active photocatalysts. Catalysts with various favorable properties, like showing high visible-light absorption and having huge surface areas, better charge separation abilities and long-term photostabilities, are confirmed to be the best in the field of photocatalysis. However, it is rather difficult to attain all of the above features from one component.

Inspired by current areas of research, we have designed a smart visible-light active photocatalyst and focused on the stabilities and activities of AuPd alloy NPs with various ratios of Au to Pd, as well as GO/LDH nanocomposites individual decorated with Au and Pd, for photocatalytic Suzuki coupling reactions. The surface coordinated APTS ((aminopropyl)triethoxysilane) groups can effectively control the uniform distribution of alloyed metal NPs over the GO/LDH surface. The AuPd alloy photocatalyst (1 : 1) gave 95.5% yield during the Suzuki coupling reaction, without any indication of leached metal alloy. The improved catalytic activity can be ascribed to contributions from each component synergistically activating the reactants in the visible region, where the large number of photo-generated electrons and holes can be utilized for the activation of iodobenzene and phenylboronic acid, respectively. This study no doubt opens up a new window onto visible-light driven materials for organic coupling reactions.

Experimental

Materials and reagents

All the chemicals used, such as potassium permanganate ($KMnO_4$), sodium nitrate ($NaNO_3$), hydrochloric acid (HCL), sulphuric acid (H_2SO_4), sodium hydroxide (NaOH), hydrogen peroxide (H_2O_2), graphite powder, auric acid ($HAuCl_4$), palladium(II) chloride ($PdCl_2$), iodobenzene, phenylboronic acid, and potassium carbonate (K_2CO_3), were purchased from Merck. The starting materials for layered double hydroxide (LDH) preparation, i.e., nitrate salts ($Cr(NO)_3 \cdot 9H_2O$ and $Zn(NO)_3 \cdot 6H_2O$), were obtained from Sigma Aldrich. The above reagents were all used as received in the performed experiments.

Preparation of the ZnCr LDH/GO nanocomposite

The popular Hummers' method is followed to prepare graphene oxide from graphite powder. The composite, i.e., LDH/GO, was fabricated via the in situ nucleation of the ZnCr LDH from the respective metal precursors over the surface of GO sheets. In detail, a weighed amount of as-prepared GO was added to 100 mL of DW (deionised water), subjected to ultra-sonication (1 h) and further stirred for half an hour

This journal is © The Royal Society of Chemistry 2019

Catal. Sci. Technol., 2019, 9, 4678–4692 | 4679

under ambient conditions. 40 mL of a 3 : 1 molar ratio (Zn^{2+} : Cr^{3+}) mixed metal solution of $Zn(NO_3)_2 \cdot 6H_2O$ and $Cr(NO_3)_3 \cdot 9H_2O$ in DW was prepared and 0.2 M NaOH solution was also prepared. Then, both the alkaline and metal nitrate (Zn^{2+} : Cr^{3+}) solutions were added simultaneously to the above-prepared GO suspension dropwise. Then the pH of the solution was carefully maintained at 10 throughout composite (LDH/GO) formation. Further, the obtained slurry was placed under stirring for 4 h, followed by heating for nearly 8 h at 90 °C. Ultimately, the suspension (grey colour) was filtered and rinsed several times with DW and kept in a hot air oven for one day at 100 °C. The as-formed material is designated as the LDH/GO composite.

Synthesis of GO/LDH@APTS

1 g of GO/LDH was suspended in a round bottom flask with 30 mL of toluene. Then, 5 mL of APTS ((aminopropyl)triethoxysilane) was added slowly to the above suspension and it was refluxed for 6 h. After that, the above solution was filtered and rinsed frequently with DW and ethanol. Subsequently, the above sample was dried in an oven overnight at 70 °C. The formed sample is referred to as the GO/LDH@APTS composite.

Synthesis of the GO/LDH@AuPd hybrid nanocomposite

1 g of the above-prepared GO/LDH@APTS composite was suspended in ethanol (50 mL) and subjected to sonication (30 min). To the as-formed faint black suspension, equal volumes (5 mL) and molar strengths (0.01 M) of $HAuCl_4$ and $PdCl_2$ solutions were injected and the mixture was stirred continuously for 4 h under ambient conditions. Then the metal-including solution was exposed to a UV light source in the form of a 300 W Xe lamp (without a cut-off filter) equipped with a Lelesil quartz reactor for a time period of 3 h. The above-mentioned light-illuminated solution was centrifuged repeatedly with DW followed by ethanol before at last being dried overnight in a hot air oven at 80 °C. The as-formed dry material is denoted as Au_1Pd_1@LDH/GO. Similarly, single metal loaded LDH/GO samples, i.e., Au@LDH/GO and Pd@LDH/GO, were prepared following the same procedure as mentioned above for the bimetallic loaded LDH/GO composite but, in this case, 10 mL of either the $HAuCl_4$ (0.01 M) or $PdCl_2$ (0.01 M) metal precursor was used for the respective metal decorating of the composite. The same method was used to prepare Au_2Pd_1@GO/LDH and Au_1Pd_2@GO/LDH. A similar preparation method can also be adopted in the case of the GO@AuPd nanocomposite.

Photocatalytic Suzuki coupling reaction

In a typical Suzuki coupling reaction, 0.1 mL (1 mmol) of iodobenzene, 0.227 g (1.5 mmol) of phenylboronic acid, 5 mL of water, 15 mL of ethanol, 0.41 g (3 mmol) of K_2CO_3 and 0.01 g of catalyst were mixed together under vigorous stirring. The reaction mixture was exposed to a 300 W Xe lamp equipped with a cut-off filter ($\lambda \geq 420$ nm) under magnetic stirring for 2 h and the reaction was maintained at a temperature of 25 ± 5 °C with constant flowing water connected to a chiller (Julabo300F). After the photocatalytic reaction, the solution was centrifuged (REMI R-24) for the separation of the catalyst. The liquid phase product was analyzed via gas-chromatography (GC, Thermo scientific Trace 1110) with an FID detector using an SE-30 capillary column. In the case of using H_2O as the solvent, the product was extracted with dichloromethane prior to GC analysis. All the dark reactions were carried out in the same way as the photocatalytic reactions. Additionally, the separated catalyst was then washed several times with distilled water and ethanol, and subsequently dried under vacuum at 70 °C overnight. The collected catalyst was recycled for further reactions.

Characterization techniques

Crystallographic information relating to the as-prepared samples was analysed using a Rigaku Miniflex XRD machine with a Cu Kα (λ = 1.5418 Å) X-ray source within the scan window of 2θ = 5–80° at a scan rate of 2° min^{-1}. A JASCO FT-IR spectrometer with a frequency range of 500–4000 cm^{-1} was used for FT-IR spectral measurements with KBr as a reference. The optical behaviour of the synthesised materials, such as the UV-vis DRS and photoluminescence behaviour, was verified using a JASCO V-750 spectrophotometer and FP-8300 spectrofluorometer. A VG Microtech Multilab ESCA 3000 spectrometer equipped with an Al Kα X-ray source and a charge neutraliser was utilised to characterise XPS spectra. The Raman phonon vibrations of the samples were analysed with a Renishaw inVia Raman microscope. TEM and HRTEM characterization was undertaken with the help of a Philips TECNAI G2 instrument (200 kV accelerating voltage). Impedance (EIS) and Mott–Schottky (MS) measurements were carried out with an IVIUMnSTAT multichannel electrochemical analyser fitted with a three-electrode based system. A Lelesil Innovative-based photoreactor, fitted with a 300 W Xe light along with a UV cut-off filter and a JULABO 300F chiller, was used for the purpose of performing the photocatalytic experiments. The obtained experimental results were analysed with an Agilent technology 7890B gas chromatography system.

Results and discussion

The phase purity, structural identity and existence of Au, Pd, and bimetallic AuPd alloyed NPs were confirmed with the help of powder X-ray diffraction techniques, as shown in Fig. 1. The characteristic XRD pattern of the pure GO precursor (Fig. 1a) reveals a diffraction peak at 2θ = 11.04°, corresponding to the (001) plane, and the interlayer distance of 0.80 nm suggested the formation of oxygenic functional groups over the surface of the graphite layer.[19] All the diffraction peaks of a hydrotalcite-like material were seen at diffraction angles of 11.4°, 22.7°, 31.4° and 61°, which can be indexed to the (003), (006), (009) and (110) reflection planes of the GO/LDH nanocomposite, respectively. This result suggests the formation of a GO/LDH nanocomposite through the

4680 | Catal. Sci. Technol., 2019, 9, 4678–4692

This journal is © The Royal Society of Chemistry 2019

Fig. 1 XRD patterns of GO (a), GO/LDH (b), GO/LDH@Au (c), GO/LDH@Pd (d), and GO/LDH@AuPd (e).

effective exfoliation of GO layers with LDH sheets. The XRD pattern of the monometallic Au NPs revealed four sharp peaks at 2θ = 38.09°, 44.31°, 64.63° and 77.50°, which could be assigned to the (111), (200), (220) and (311) crystal planes, respectively (JCPDS No. 89-3697). Further, three broad peaks were seen at diffraction angles of 39.32°, 46.14° and 68.04° from the (111), (200) and (220) planes of face centred cubic Pd NPs (JCPDS No. 87-0645). In the case of the AuPd bimetallic alloy, the PXRD pattern shows 2θ values of 38.37°, 44.70°, 65.02°, and 77.82°, which can be indexed to (111), (200), (220), and (311) crystal planes, respectively. It can be observed that all the diffraction peaks of AuPd@GO/LDH were positioned in between those of the monometallic AuNP- and PdNP-modified GO/LDH composites. Additionally, all the peaks of the alloyed sample are slightly broadened and slightly shifted to higher 2θ values compared to those of monometallic AuNPs, owing to interactions with Pd atoms following the formation of the bimetallic AuPd alloy. This confirms that AuPd alloy formation takes place, rather than a mixture of mono-metals or core-shell NPs, over the facade of the GO/LDH nanohybrid, which is well supported by UV-vis and XPS characterization.[15,20]

Moreover, the average crystallite size of the noble metal NPs was calculated using the Scherrer equation by means of the full width at half maximum (FWHM) of the leading diffraction peak, *i.e.*, the (111) plane of the Au/Pd/AuPd@GO/LDH composite.[21]

$$d = k\lambda/(\beta \cos\theta)$$

where λ is the wavelength of the X-ray source (1.54 Å), β is the FWHM of the most dominant peak, k is an empirical constant (0.89), and θ is the angular location. Therefore, from PXRD analysis, the crystallite sizes were estimated to be 12.78 nm for Au@GO/LDH, 1.9 nm for Pd@GO/LDH and 2.98 nm for AuPd@GO/LDH. This decrease in the crystallite size of

the AuPd alloyed NPs compared to the monometallic Au NPs may be caused by associated lattice strain, and this again confirms the creation of bimetallic alloyed NPs. Moreover, the particle size of the AuPd alloy was measured to be ~4.2 nm (from Fig. 3f), which is comparable with the crystallite size of the AuPd alloy. However, this remarkable difference between the average particle (~4.2 nm) and crystallite (2.98 nm) sizes of the alloyed NPs indicates that the particles might consist of several crystallites, *i.e.*, individual crystallites may agglomerate to form a particle, which is in agreement with the literature.[22,23]

The optical absorption properties and band gaps of the as-synthesized nanohybrid samples were probed using a UV-vis DRS spectrophotometer. The light absorbance spectra of GO/LDH, GO/LDH@Au, GO/LDH@Pd and GO/LDH@AuPd are depicted in Fig. 2. It is seen that the GO/LDH nanocomposite shows the existence of two absorption bands at 410 nm and 565 nm. The first one is due to O 2p → Cr 3d(t_{2g}) ligand-to metal charge-transfer (LMCT) in an octahedral environment, and the second one is attributed to Cr 3d(t_{2g}) → Cr 3d(e_g) metal to metal charge transfer (MMCT) caused by the d–d transition of Cr^{+3}. Additionally, in the case of the GO/LDH nanocomposite, the band in the range of 200–350 nm may be due to LMCT, *i.e.*, from O 2p → Zn 3d and O 2p → Cr 3d(e_g).[24] It was observed that after the introduction of noble metal nanoparticles to the GO/LDH nanocomposite, the absorption edge showed a bathochromic shift compared to the parent GO/LDH. This red shift obviously demonstrates that the visible light absorption capacity is enormously increased with the loading of single noble metal or bimetallic alloyed NPs. In the case of GO/LDH@Au, a broad absorption band appeared at around 560 nm, rather than the LSPR peak at 530 nm. This may be due to the fact that the plasmon peak of gold overlaps with the MMCT band of the GO/LDH composite material causing a broad band. Moreover, no

Fig. 2 UV-vis spectra of the as-synthesized samples illustrating the surface plasmon resonance effect.

This journal is © The Royal Society of Chemistry 2019

Catal. Sci. Technol., 2019, **9**, 4678–4692 | **4681**

characteristic peak was observed in the case of the Pd-loaded GO/LDH composite. However, in the case of the AuPd alloyed sample, the Au SPR band disappeared, which is due to the existence of a group 10 (*i.e.*, $d^8 s^2$) metal in the bimetallic NPs, which suppresses the SPR energy of the group 11 (*i.e.*, $d^{10} s^1$) metal.[25,26] This implies the creation of AuPd bimetallic alloyed NPs.

Furthermore, the band gap energies were determined from the Kubelka–Munk absorbance and Tauc plots. It was observed that the GO/LDH nanocomposite showed an indirect transition and the estimated band gap energy value was 2.47 eV, which matches well with the published literature.[24]

The TEM images of GO/LDH@AuPd in Fig. 3 display the novel hybrid structure of the alloyed nanocomposite, where the distribution of nanosized spherical AuPd bimetallic alloy particles was observed over the platform of the 2D matrix (GO/LDH). This offers advanced properties, contributing towards the enhancement of the photocatalytic performance of the composite. It is clearly seen that the AuPd alloyed NPs are strongly wrapped in gauze-like crumpled and rippled GO sheets, as shown in Fig. 3(a), and some of the bimetallic alloyed AuPd NPs can be seen to be uniformly distributed on the surface of the ZnCr LDH nanosheets, as shown in Fig. 3(b) and (c). Again, Fig. 3(b) clearly suggests that the nucleation of LDH occurs over the GO surface and further LDH sheets get bound to the GO surface through electrostatic interactions, confirming the strong interactions between GO and LDH due to their oppositely charged frameworks. Moreover, the existence of AuPd alloyed NPs is verified through the HRTEM image shown in Fig. 3(d). Two different lattice fringes were observed in the alloyed metal NPs; the lattice fringes with interplanar spacings of 0.228 nm and 0.236 nm correspond to the (111) crystallographic planes of the Pd and Au fcc structures, respectively. Additionally, the *d*-spacing of 0.20 nm is due to the (012) crystallographic plane of pure LDH, which matches well with previous reports.[27] The corresponding planes and diffraction rings can be observed in the SAED pattern shown in Fig. 3(e). The SAED pattern displays a number of intense spots in a random way; these can be allocated to the fcc crystalline structure of the alloyed NPs. The observed interplanar spacing values, supporting the existence of Au and Pd NPs, are very consistent with the XRD data and similar to the previously reported literature.[11] Further, the particle size distribution graph shows that the average diameter of the bimetallic AuPd alloyed NPs is calculated to be 4.2 ± 1.5 nm, as shown in Fig. 3(f). In order to confirm the different element content values in the GO/LDH@AuPd photocatalyst, we obtained an energy dispersive X-ray spectroscopy (EDS) mapping image, as shown in Fig. 3(g), which demonstrates the existence of Au, Pd, Zn, Cr, C, O, N and Si components in the sample. This confirms the presence of the APTS group in the sample.

To identify the chemical compositions, the oxidation states of the included metals and the electronic contributions of the LDH and AuPd in the GO/LDH@AuPd nano-composite, X-ray photoelectron spectroscopy (XPS) analysis was performed and the obtained data is depicted in Fig. 4. The survey spectrum analysis in Fig. 4(a) shows the existence of Zn, Cr, Au, Pd, O and C components in the hybrid nano-composite. Fig. 4(b) presents the deconvoluted C 1s spectrum of GO/LDH@AuPd, where the peaks located at about 284.54 and 288.44 eV are attributed to sp^2 graphitic carbon and carbon atoms bonded with oxygen atoms (–COOH groups), respectively.[28] Additionally, the O 1s spectrum is deconvoluted into two signals, *i.e.*, 530.37 and 531.92 eV, which are associated with the bridging OH and terminal OH groups of LDH, respectively.[29] As shown in Fig. 4(d) and (e), the signals centred at about 1022.8 and 1045.8 eV represent the Zn $2p_{3/2}$ and Zn $2p_{1/2}$ spin states, whereas signals from Cr $2p_{3/2}$ and Cr $2p_{1/2}$ were noticed at 578.09 and 587.2 eV in the GO/LDH@AuPd sample. It is found that the binding energy values of the composite LDH are slightly higher in energy than those of our previously reported literature binding energy values of pure LDH (Zn $2p_{3/2}$: 1022.7 eV; Zn $2p_{1/2}$: 1045.0 eV; Cr $2p_{3/2}$: 577.6 eV; and Cr $2p_{1/2}$: 586.38 eV).[30] The shifting of the binding energies demonstrates a reduction of the electron density around Zn and Cr in GO/LDH@AuPd owing to the transfer of electrons from the LDH to the directly attached AuPd alloy NPs and also to those anchored on the GO surface *via* the π-conjugated skeleton of the GO sheets. This further confirms the strong interactions between the AuPd alloy and the support (GO and LDH) in the GO/LDH@AuPd sample.[31] Moreover, in the case of the GO/LDH@AuPd sample, the binding energies centred at 82.5 and 87.4 eV are allotted to electronic transitions (Au $4f_{7/2}$ and Au $4f_{5/2}$) and the peaks at 335.6 and 340.9 eV are assigned to the Pd $3d_{5/2}$ and Pd $3d_{3/2}$ regions, respectively, suggesting the presence of metallic Au^0 and Pd^0 species, respectively. However, in the case of the single metal loaded LDH, the signals at around 83.8 and 87.5 eV are assigned to Au$4f_{7/2}$ and Au$4f_{5/2}$,[29] and the peaks at 335.4 and 340.7 eV are assigned to the Pd$3d_{5/2}$ and Pd$3d_{3/2}$ energy levels, respectively.[32] It was spotted that in the AuPd alloyed composite, the transition of Au 4f shows a negative shift and that of Pd 3d shows a positive shift compared to the single metal NPs, relative to our previous report. These above results reveal that charge transfer occurs from Pd to Au, *i.e.*, charge transfer takes place from the lower electronegativity of Pd (2.20) to the higher electronegativity of Au (2.54). The above electronic interactions also demonstrate the formation of the AuPd alloyed sample.

The Raman polarization bands of the parent graphene oxide (GO), *i.e.*, the G (E_{2g}) and D (A_{1g}) bands, could be clearly visualised at 1587 and 1344 cm^{-1}, respectively, because of two symmetric levels, the central zone and *k*-point phonons, as shown in Fig. 5. More importantly, the hump depicting the G mode of the Raman vibrations highlights the sp^2 carbon skeleton in the GO sheets, which are formed *via* the reduction of oxygen-containing groups, whereas the D band of GO indicates the occurrences of defects. Interestingly, the red shift in the wavenumbers of both the G (1587 to 1599 cm^{-1})

Fig. 3 (a–c) TEM and (d) HRTEM images, (e) an SAED pattern, (f) the particle size distribution and (g) the EDX spectrum of the GO/LDH@AuPd nanocomposite.

This journal is © The Royal Society of Chemistry 2019

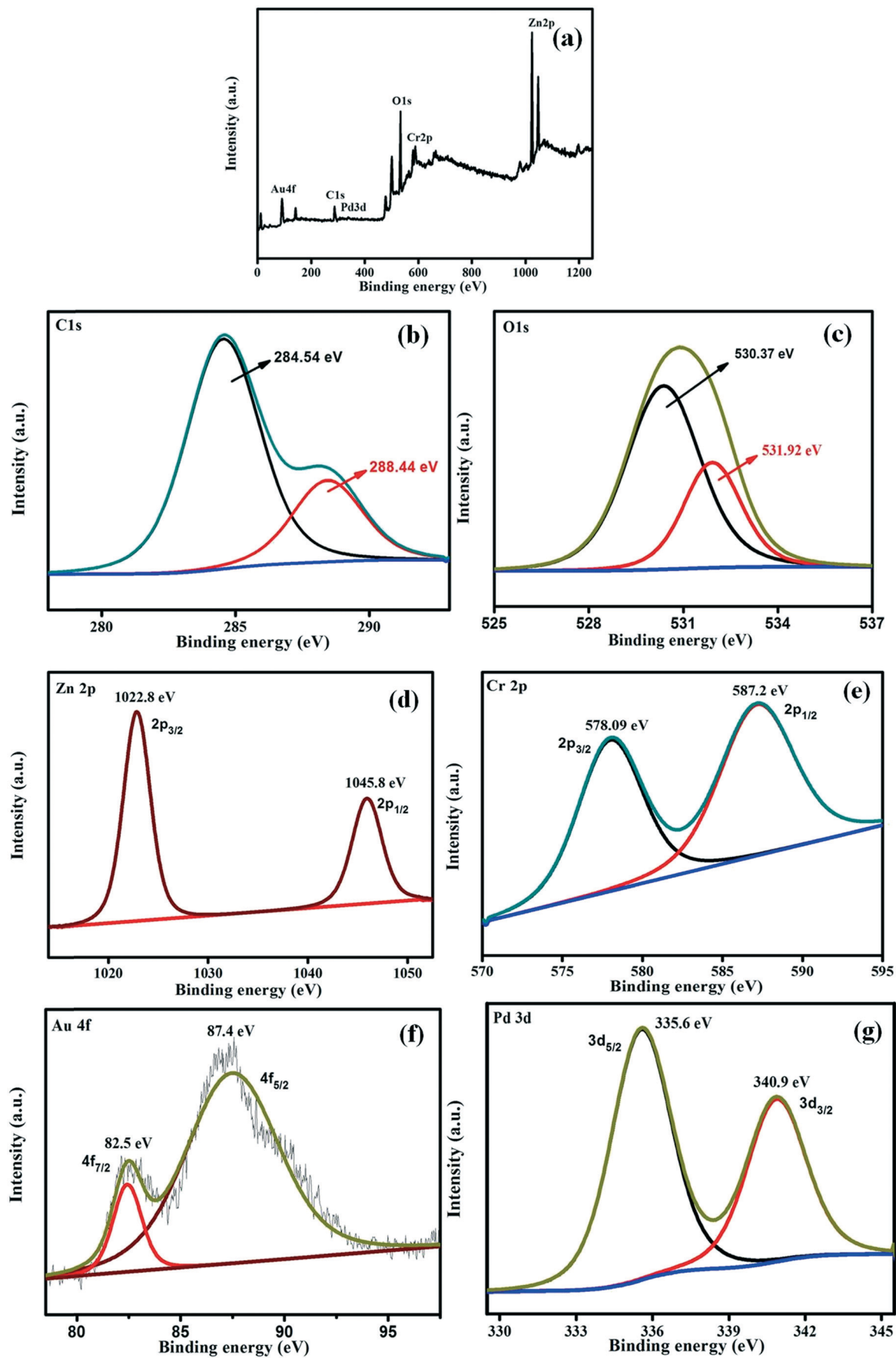*Catal. Sci. Technol.*, 2019, **9**, 4678–4692 | **4683**

Fig. 4   XPS analysis of the GO/LDH@AuPd catalyst: (a) total survey scan, (b) C 1s, (c) O 1s, (d) Zn 2p, (e) Cr 2p, (f) Au 4f and (g) Pd 3d.

and D (1344 to 1350 cm^{-1}) phonon bands of GO in the GO/LDH hydride suggests the successful reduction of GO to RGO *via* the photoreduction method. Further, the band intensity (D to G) ratio, *i.e.*, I_D/I_G, of GO illustrates critical ideas about the defects and distortions in the carbon skeleton that play a vital role in enhancing the catalytic ability of the photocatalyst. Moreover, the shift in the band intensity ratio (I_D/I_G) from 0.98 in neat GO to 1.08 in the LDH/GO composite indicates the successful reduction of GO to rGO and also the creation of defects in the GO sheets. These defects or vacancies on the GO surface act as nucleation sites for the LDH. Additionally, one more shoulder band, located at about 2684 cm^{-1}, represents the 2D band that provides idea about the formation of the single layer structure[33] and defect sites (inset of Fig. 5). All of the above observations suggest the successful reduction of GO to rGO (LDH/GO) using the followed photoreduction method and also indicate the strong chemical interactions between GO and the LDH that prevent the stacking of GO sheets. The above claims clearly justify the successful photoreduction of GO and the development of the LDH/GO hybrid.

The photocatalytic performance largely depends upon the behaviour of charge carriers, *i.e.*, charge separation and migration, within the photocatalyst, and the effectiveness of these physical phenomena are well characterized through PL and EIS analysis (Fig. 6). Conceptually, the intensity of a PL peak varies directly with the recombination rates of excitons, *i.e.* intense peaks mean faster recombination and *vice versa*. Similarly, the diameter of the arc obtained from a Nyquist plot after EIS measurements (Fig. 6a) gives information regarding the electrode/electrolyte interface charge transfer resistance; a smaller arc radius implies better conductivity, faster charge transfer and low electron–hole recombination and, hence, excitons with longer life spans. A bigger semicircle indicates faster recombination and poor electrical conduc-

tance. Again, the slope of the line in the higher frequency zone of the graph represents the Warburg resistance, which represents the ion diffusion process; a straighter line suggests a more smooth diffusion mechanism. In the performed PL study (λ_{ex} = 360 nm) of the GO/LDH@AuPd and GO/LDH composites, the observed emission peak for GO/LDH@AuPd is of low intensity compared to GO/LDH, which proves better charge carrier separation in the former and, hence, superior catalytic activity (Fig. 6b). Additionally, the peaks positioned at 468 nm and 492 nm indicate defect sites and band-to-band emission, respectively. Moreover, the strong band observed in the region of 415–435 nm was due to the trapping of surface excitation charge. The lowering of the PL peak intensity in the case of the bimetallic alloy modified GO/LDH composite is attributed to the Au–Pd loading. Furthermore, the EIS analysis carried out within a frequency range of 10^1–10^6 Hz clearly supports the effective electron–hole separation and migration efficiency of the GO/LDH@AuPd photocatalyst, with a smaller Nyquist semicircle and a straighter Warburg line compared to GO/LDH.

Photocatalytic activity towards the Suzuki coupling reaction (SCR)

The photocatalytic activity of the AuPd alloyed nanocatalyst with enriched electron density under a visible light beam can also be shown towards the SCR between iodobenzene (IB) and phenylboronic acid (PBA). In order to analyse the role of the active metal, an initially bare GO/LDH sample was tested for the coupling reaction, as indicated in Table 1. In the absence of AuPd alloy, a trace amount of biphenyl yield was achieved after 3 h of visible light illumination. In contrast, the loading of noble metals can drastically change the catalytic activity. Thus, we confirmed that the alloyed metal can drastically result in electron density enhancement and also activate iodobenzene for the coupling reaction.

To discuss the synergistic effects of Au and Pd, a series of experiments was also performed and the results are summarized in Table 1. In the case of the GO/LDH@Pd catalyst, the yield rises gradually and reaches up to 35.3%, whereas in the case of the GO/LDH@Au catalyst, the yield of biphenyl was 16.4% after 2 h of visible light illumination. The yield of biphenyl was higher in the case of GO/LDH@Pd than GO/LDH@Au. This indicates that Pd is the active component but has a low responsiveness to light during the coupling reaction. Here, GO/LDH@AuPd provides the maximum biphenyl yield of 99.5% under the same reaction conditions for 2 h compared with the individual mono-metals. This yield was even 1.9 times the overall yield of GO/LDH@Au and GO/LDH@Pd, demonstrating that the AuPd alloyed sample showed higher catalytic efficiency for the Suzuki coupling reaction under mild conditions. This was due to plasmonic Au synergistically improving the aptitude of Pd collectively with GO/LDH to boost the catalytic activity for the SCR in less time.

To verify the function of the LDH in the GO/LDH@AuPd nanocomposite, a coupling reaction was carried out
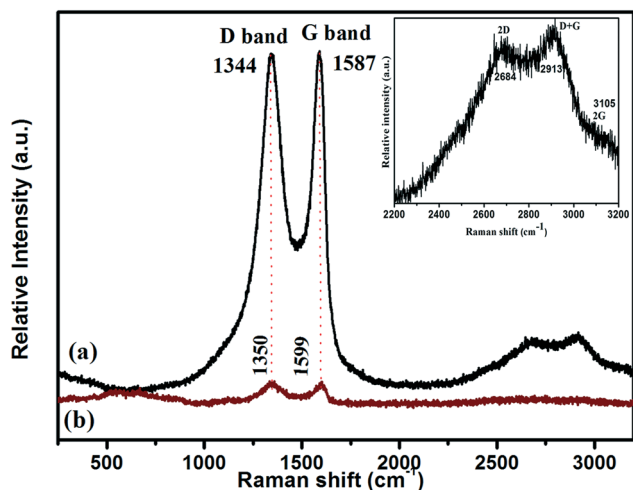

Fig. 5 Raman spectra of samples: (a) GO and (b) the GO/LDH@AuPd nanocomposite. The inset figure is an enlarged portion of the Raman spectrum of the GO/LDH@AuPd nanocomposite.

Fig. 6 (a) Electrochemical impedance spectra (Nyquist plots) and (b) PL spectra of parent GO/LDH and GO/LDH@AuPd.

separately with the catalyst GO@AuPd, and the reaction results are given in Table 1. The results indicate that in the absence of the LDH, a small amount of biphenyl yield was achieved after 2 h of visible light illumination compared to the GO/LDH@AuPd nanocomposite. Thus, this confirms that the presence of the LDH can enhance drastically the photocatalytic activity due to its visible-light active semiconducting properties. Thus, we confirmed that the GO/LDH@AuPd nanocomposite can drastically result in electron density enhancement and can also activate iodobenzene for the coupling reaction.

Furthermore, the effects of the solvent also play a very crucial role in the organic transformation, and the obtained results regarding the reaction rate are summarized in Table 1. The reaction was carried out separately with various solvents (such as DMF/H_2O (3:1), EtOH/H_2O (3:1) and toluene/H_2O (3:1)) to study the effects of solvent polarity towards the Suzuki coupling reaction. The reaction results can be explained on the basis of

polarity (dielectric constant (ε) = 36.7 for DMF, 24.3 for ethanol, and 2.4 for toluene). Ethanol is shown to be a good reaction medium for this reaction, whereas non-protic and less polar solvents, including toluene, are not as suitable for the SCR. Polar aprotic solvents like DMF give a lower yield of the coupling product. Here, ethanol shows better activity than DMF due to its amphiprotic nature.[34] The better activity of the mixed solvent (*i.e.* EtOH/H_2O) may be because of the improved solubilities of the bases and the reactants, because the capacity to dissolve bases in water to stimulate phenylboronic acid can increase the rate of the reaction in the aqueous medium.

To further investigate the spatial arrangement of Au and Pd and the synergistic catalytic effects, the SCR reaction was also catalyzed with a blended catalyst in the form of GO/LDH@Au and GO/LDH@Pd under similar reaction conditions. The mixed alloy catalyst and the blended catalyst showed zero catalytic activity for the SCR under dark conditions (Fig. 7a). This is due to the fact that in the absence of

Table 1 The effect of various catalysts towards the Suzuki cross-coupling reaction

Catalyst	Time (h)	Solvent	Yield (%)	Selectivity (%)
GO/LDH	3	EtOH–H_2O (3:1)	Trace	—
GO/LDH@Au	2	EtOH–H_2O (3:1)	16.4	>99
GO/LDH@Pd	2	EtOH–H_2O (3:1)	35.3	>99
GO@AuPd	2	EtOH–H_2O (3:1)	87	>99
GO/LDH@AuPd	2	EtOH–H_2O (3:1)	99.5	>99
GO/LDH@AuPd	2	DMF–H_2O (3:1)	82	>99
GO/LDH@AuPd	2	Toluene–H_2O (3:1)	46	>99

Reaction conditions: iodobenzene, 1 mmol; phenylboronic acid, 1.5 mmol; photocatalyst, 0.01 g; base: K_2CO_3, 3 mmol; 20 mL of solvent (V:V = 3:1); 25 ± 5 °C for 2 h.
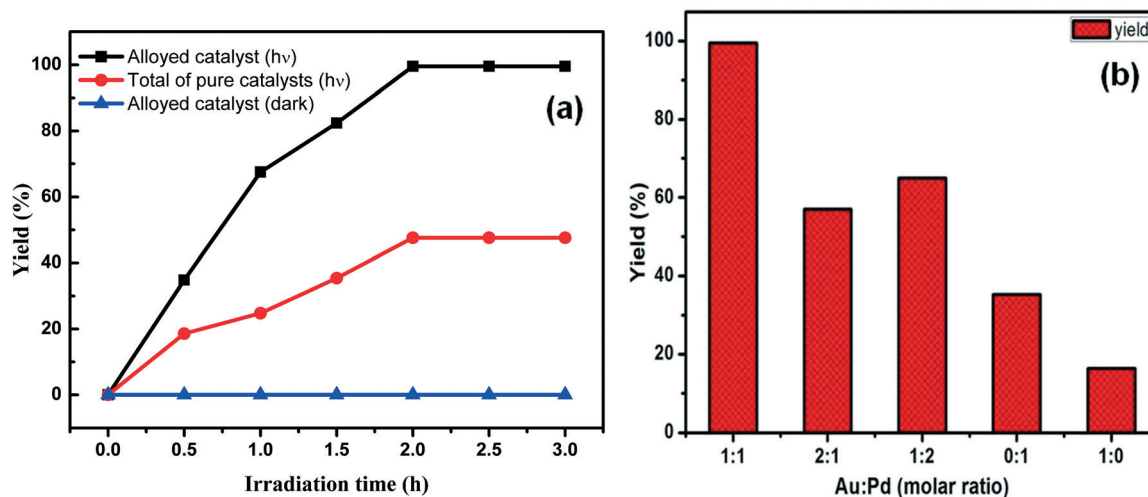
Fig. 7 Biphenyl yield (a) using different spatial arrangements of catalyst and (b) depending on the metal ratio of Au : Pd.

light there is poor electron density on Pd. Therefore, charge transfer from Pd does not takes place for the activation of IB. However, in the presence of visible light for 2 h, the product yield of the blended (total of pure) catalyst reached only 47.6%, which almost matched the total of the individual yields catalyzed by GO/LDH@Au and GO/LDH@Pd. Therefore the total of the pure catalysts shows no increase in catalytic activity, which specified that there is no charge transfer involved between Au and Pd because of the individual spatial arrangement of the two noble metals.

We have figured out the importance of the chemistry relating to the ratio of noble metal loading and how it affects photocatalytic activity, as shown in Fig. 7b. We have studied different ratios of Au to Pd nanoparticles in the composite and found that at a certain ratio (1 : 1) AuPd bimetal formation takes place, and this bimetallic modified catalyst shows better performance. However, an increase in the concentration of single metal Au or Pd (i.e., at a ratio 1 : 2 or 2 : 1) induced a decrease in catalytic activity, which may be due to the broken nanostructure of the perfect bimetallic alloy at higher atomic ratios of Au : Pd; in other words, we can say that surface segregation is a natural phenomenon in bimetallic alloys. Therefore, with a decrease in the content of one metal, another active domain metal may aggregate, leading to a reduction in the catalytic activity.

To further draw attention to the superiority of the present work, a comparison data (Table 2) is given that shows a num-

ber of other similar types of reported works; this shows that the catalytic activity of our work is superior to other published literature results under mild conditions.

Formation mechanism of the alloyed catalyst

The positively charged surface of the LDH gets attached to the negatively charged GO sheet electrostatically, resulting in the formation of a stable GO/LDH hybrid. It is quite easy to switch the surface properties of the formed hybrid, as both the combined entities are rich in oxygen-containing functional groups, i.e., epoxy, carbonyl and hydroxyl groups are readily present in GO and hydroxyl groups are present in the LDH. From our previous report, we revealed that organic moieties get strongly attached to LDH surfaces through surface hydroxyl groups via covalent bonds (i.e., Si–O–M bond).[35] Further, the amine-functionalised composite that is formed via the interaction of APTS ((aminopropyl)trimethoxysilane) and the hydroxyl groups of the LDH provides necessary binding sites for the nucleation of stable Au–Pd bimetallic alloy nanoparticles. Two things work simultaneously in this synthesis method: first, the hydroxyl groups on the support act as a bed for alloy deposition; and second, ATPS prevents agglomeration and, hence, stabilises the Au–Pd bimetallic alloy compared to other preparation techniques.

The science behind the decoration of Au–Pd bimetallic alloy nanoparticles on the surface of GO/LDH is shown in

Table 2 The photocatalytic ability of our system compared to other systems

Sample	Time (h)	Amount of catalyst	Yield (%)	Light source	Light intensity	Reference
AuPd/GO/LDH	2	10 mg	99.5	300 W Xe lamp	150 mW cm^{-2}	This work
Pd/Au/PN-CeO$_2$	5	15 mg	98.8%	Xe lamp (150 W) (cut off <400 nm)	—	14
Au–Pd alloy	6	50 mg	96%	Halogen lamp (Nelson, λ = 400–750 nm)	0.5 W cm^{-2}	15
Au–Pd/TiO$_2$	5	0.0002 mmol Pd	98%	5 W blue LED lamp	—	16
Au–Pd@ZrO$_2$	6	50 mg	96%	500 W halogen lamp (Nelson, λ = 400–750 nm)	0.30 W cm^{-2}	40
Pd hexagonal nanoplates	3	15 mg	92%	Xenon lamp, visible to near-infrared	—	43

Scheme 1 Mechanism of the formation of the GO/LDH@AuPd photocatalyst.

Scheme 1. The gold precursor (HAuCl₄) splits into H⁺ and AuCl₄⁻ ions, and the formed H⁺ ions interact with the amine groups of functionalised GO/LDH resulting in the formation of ammonium ion. This makes the functional group (APTS) attached to the surface positively charged, so the negative ion (AuCl₄⁻) can easily bond to the LDH surface. Further, both metal precursors are added at the same time, but AuCl₄⁻ interacts first with the positively charged LDH, as Pd exists in the form of positive ions. However, the Pd ions now get strongly bound through metallic bonds to the negatively charged gold particles, resulting in the formation of a stable AuPd bimetallic alloy. Further, *via* a galvanic exchange reaction pathway, the chemical reduction priority between AuCl₄⁻ and Pd²⁺ ions is decided, *i.e.*, Au³⁺ with its high redox potential is reduced first followed by Pd²⁺ ions *via* the photoreduction technique (as the reduction potential values are $E_{Au^{3+}/Au}^0$ = 1.5 V and $E_{Pd^{2+}/Pd}^0$ = 0.83 V *vs.* NHE).[36] Additionally, based on the electronegativity concept, electron transfer occurs from the lower electronegativity Pd atom (2.20) to the higher electronegativity Au atom (2.54). Therefore, electrons will flow from Pd to Au until equilibrium is reached in the AuPd alloy structure, as shown in Scheme 2, which matches well with the XPS data. Moreover, the high surface area of the GO

nanosheets provides good dispersion of the supported bimetallic alloy NPs, which favours the exposure of more active sites for photocatalytic reactions. Interestingly, due to the even decoration of the bimetallic alloy on the GO/LDH surface, the catalytic efficiency of the fabricated ternary hybrid becomes significantly enhanced.

Formation mechanism of RGO and the metal NPs

Upon illumination by light (300 W Xe lamp without a cut-off filter), the photogenerated holes from the LDH are scavenged to form ethoxy radicals in the presence of ethanol. At that time, the accumulated photogenerated electrons are transported across the GO sheet to reduce functional groups present on GO to form RGO; they also combine with metal ions (Pd²⁺ and AuCl₄⁻) to produce metal NPs (Pd and Au).[37] Therefore, this process of synthesis is followed by a co-reduction technique. This type of synthesis is quite important, as both the metal and GO are reduced in a single step, which is similar to our recently published paper.[12]

Mechanism of the Suzuki coupling reaction (SCR) over the GO/LDH@AuPd catalyst

The projected mechanistic pathway justifying the enhanced photocatalytic performance of the fabricated bimetallic-GO/LDH composite (GO/LDH@AuPd) toward the SCR (iodobenzene and phenylboronic acid) is detailed below (Scheme 3). The triggered visible light assisted SCR involves the cleavage of the C–I bond in iodobenzene and the stimulation of its coupling partner (phenylboronic acid), which ultimately results in biphenyl formation. The above process proceeds *via* (a) oxidative addition, (b) transmetallation and (c)

**Scheme 2** Schematic diagram showing the formation of the alloy.

Scheme 3 A possible reaction mechanism where iodobenzene is activated *via* electrons on the Pd NPs and the coupling partner phenylboronic acid is activated *via* holes from the LDH. The redox activated groups then get together to couple and form the final product.

reductive elimination. A full overview of how the visible light stimulated SCR between iodobenzene and phenylboronic acid is performed is described as follows. As bimetallic alloy formation takes place over both the LDH and GO surfaces, the SCR commences on both 2D surfaces, which leads to higher catalytic activity. Pd from the alloy acts as the main reaction site, whereas Au has nothing to do with the reaction; its only role is to absorb visible light through the LSPR effect,[38,39] resulting in the generation of hot electrons, which later on are injected into its alloy counterpart Pd, *i.e.*, Au loses d-electrons and Pd gains d-electrons, and these d-electrons are vital in the processes of chemisorption and catalysis. Moreover, the hot electrons produced by the gold

NPs also have the chance to be inserted into the CB of the LDH. However, the hot electrons are more easily introduced into Pd because of the equilibrium chemical potentials of electrons in Au and Pd NPs. This promising electron movement has also been confirmed both through earlier research and theoretical calculations.[40]

The electrons accumulated on Pd are used in the coupling reaction resulting in a decrease in the electron density over Pd, which is supplemented by the generated hot electrons. This electron transfer causes the generation of more Au^+ ions that need to be converted to metallic gold (Au), otherwise the catalytic efficiency of the composite will be reduced. Now the role of the LDH component of the composite comes into play, as we know that the LDH harnesses visible light. Therefore, under light illumination the LDH get photoexcited and transfers some of its photoelectrons directly to the alloy (the Au/Pd alloy formed on the LDH surface) and a few photoelectrons *via* GO to the alloy (the bimetallic alloy nucleated on the GO surface); these ultimately regenerate Au from Au^+ and so the catalytic activity is maintained. Now, under visible light illumination, the Au NPs (present on the LDH and GO) capture irradiated photons and produce hot electrons *via* the LSPR phenomenon. These electrons then migrate to the Pd nanocatalyst (both over the LDH and GO) and enrich its electron count. Further, Pd with its high electron concentration sensitizes the iodobenzene C–I bond and initiates the first step of the SCR, *i.e.*, oxidative addition resulting in the formation of $ArPd^{II}I$ species. At the same time, exciton
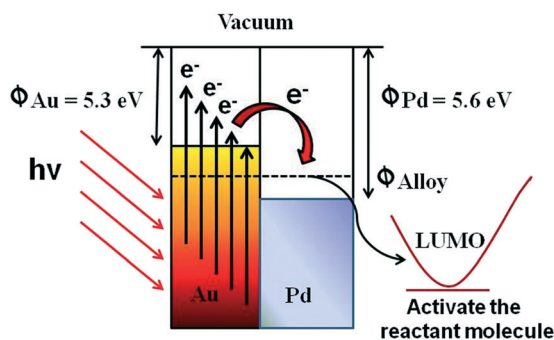
Scheme 4 The plasmonic behaviour of the AuPd alloyed NPs towards the activation of the reactant molecules.
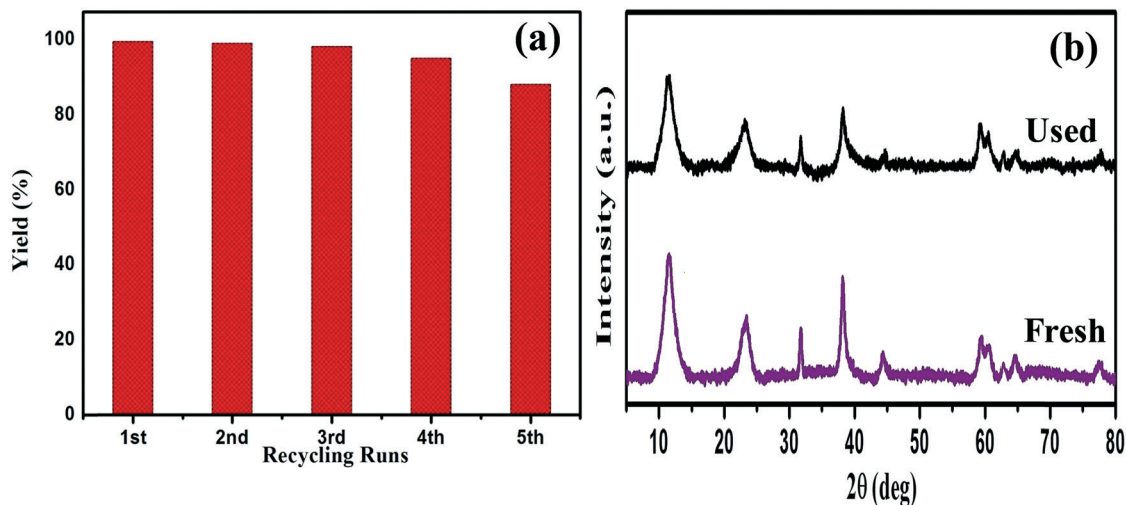
Fig. 8 (a) A reusability study over five successive runs of the SCR using the GO/LDH@AuPd nanocomposite, and (b) XRD patterns of GO/LDH@AuPd before and after the photocatalytic reaction.

generation takes place on the LDH *via* absorbing irradiated photons. Moreover, the accumulated holes in the valence band (VB) of the LDH activate the coupling partner of the reaction, *i.e.*, phenylboronic acid, through breaking the C–B bonds.[41] Likewise, the photoexcited electrons in the conduction band of the LDH get injected to directly attached Au and through the GO π-skeleton to Au in the bimetallic framework, where Au^+ is converted to Au and is ready to produce hot electrons. In the final step, the oxidised phenylboronic acid (in the VB of the LDH) moves to Pd territory, where the previously activated iodobenzene is located ($ArPd^{II}I$), and the coupling reaction occurs, producing biphenyl.

Moreover, in order to prove this mechanism, we have carried out scavenger testing, to investigate the importance of the active species (h^+ and e^-) in the photocatalytic Suzuki coupling reaction. Scavenger experiments were carried out by taking DMSO as an electron trapping agent and citric acid as a hole scavenger, separately under the same reaction conditions; this resulted in very minimal product yields, *i.e.*, 23% and 17%, respectively, as proved *via* GC analysis. Moreover, after capturing both electrons and holes upon the addition of both scavengers, only trace amounts of the biphenyl product were obtained. These experiments led to the conclusion that both the holes and electrons are important for activating phenylboronic acid and iodobenzene, respectively, for the formation of the target product. Similar types of experiments have been carried out by Wang *et al.*[42]

Additionally, Scheme 4 explains the detailed plasmonic behaviour of AuPd alloyed NPs towards the activation of the reactant molecules. As is well known, the work function of Pd (Φ_{Pd} = 5.6) is slightly larger than the work function of Au (Φ_{Au} = 5.3). Then, following the irradiation of the alloyed nanostructure by visible light (when the two metals are in contact with each other), energetic electrons will flow from Au to Pd in order to achieve equilibrium (Φ_{alloy}), creating an equal chemical potential gradient. As a result of this charge

redistribution, Pd atoms become electron rich and Au atoms become electronically deficient. This heterogeneity in charge distribution enhances the interactions between AuPd alloyed nanoparticles and the reactant molecules (*i.e.*, iodobenzene). Thus, the bimetallic plasmonic AuPd is otherwise known as a plasmonic hybrid photocatalyst.

Stability and reusability

Durability and reusability are generally essential aspects of heterogeneous photocatalysts. After the photocatalytic Suzuki coupling reaction, the AuPd@GO/LDH catalyst was recovered from the reaction mixture by means of centrifugation and recycled for use under similar reaction conditions. As illustrated in Fig. 8(a), the photocatalyst was used to perform five successive repeat cycles without any significant decrease in yield in the coupling reaction. This demonstrates the reusable nature of the coupled reaction system under mild conditions. Moreover, Fig. 8b shows that there are no noticeable changes in the XRD peak before and after the catalytic cycling. The unaltered crystal lattice of the used AuPd@GO/LDH photocatalyst illustrates its stability.

Conclusions

With the consideration of enhancing photocatalytic activity, here the loading of bimetallic AuPd NPs on a GO/ZnCr LDH hybrid support has been suggested. This hybrid support has materialized as a novel star material and has been demonstrated to show healthy chemical surroundings for the nucleation and crystal growth of active AuPd alloyed species with combined nanoarchitecture effects. The alloy nature, crystal structure and morphology of the obtained hybrid nanoarchitectured GO/LDH@AuPd composite were characterized *via* various sophisticated techniques. Harnessing the plasmon active Au metal with Pd promotes a solar to chemical energy conversion process. Such a blended architecture

4690 | *Catal. Sci. Technol.*, 2019, **9**, 4678–4692

This journal is © The Royal Society of Chemistry 2019

enhances the individual roles of the components in the photocatalytic process. The presence of a visible-light active support plays a vital role in increasing the electron density over Pd atoms to activate iodobenzene, while the remaining holes in the LDH stimulate the coupling partner phenylboronic acid for the Suzuki coupling reaction. This multifunctional photocatalyst, associated with the full utilization of photogenerated electrons and holes, inspires elevated photocatalytic activity. The durability of the photocatalyst has also been verified *via* performing five consecutive runs without any clear loss of activity. We expect that further exploitation is required for the direct harvesting of visible light by hybrid nanocomposites for other photocatalytic organic transformation reactions.

Conflicts of interest

There are no conflicts of interest.

Acknowledgements

References

1 L. Mohapatra and K. M. Parida, *J. Mater. Chem. A*, 2016, 4, 10744–10766.

2 S. Kumar, M. A. Isaacs, R. Trofimovaite, L. Durndell, C. M. A. Parlett, R. E. Douthwaite, B. Coulson, M. C. R. Cockett, K. Wilson and A. F. Lee, *Appl. Catal., B*, 2017, 209, 394–404.

3 B. Li, Y. Zhao, S. Zhang, W. Gao and M. Wei, *ACS Appl. Mater. Interfaces*, 2013, 5, 10233–10239.

4 J. Xu, L. Luo, G. Xiao, Z. Zhang, H. Lin, X. Wang and J. Long, *ACS Catal.*, 2014, 4(9), 3302–3306.

5 J. Xu, S. He, H. Zhang, J. Huang, H. Lin, X. Wang and J. Long, *J. Mater. Chem. A*, 2015, 3(48), 24261–24271.

6 S. Ren, R. Tiruvalam, H. Qian, N. Dimitratos, L. Kesavan, C. Hammond, J. A. Lopezsanchez, R. Bechstein, C. J. Kiely and G. J. Hutchings, *ACS Nano*, 2012, 6, 6284.

7 J. Zhang, Y. Lu, L. Ge, C. Han, Y. Li, Y. Gao, S. Li and H. Xu, *Appl. Catal., B*, 2017, 204, 385–393.

8 Y. Zhang, N. Zhang, Z.-R. Tang and Y.-J. Xu, *J. Phys. Chem. C*, 2014, 118, 5299–5308.

9 G. Darabdhara, P. K. Boruah, P. Borthakur, N. Hussain, M. R. Das, T. Ahamad, S. M. Alshehri, V. Malgras, Y. Yamauchi, K. C and W. Wu, *Nanoscale*, 2016, 8, 8276–8287.

10 G. Darabdhara, M. A. Amin, G. A. M. Mersal, E. M. Ahmed, M. R. Das, M. B. Zakaria, V. Malgras, S. M. Alshehri, Y. Yamauchi, S. Szuneritsj and R. Boukherroub, *J. Mater. Chem. A*, 2015, 3, 20254–20266.

11 Z. Wang, Y. Song, J. Zou, L. Li, Y. Yu and L. Wu, *Catal. Sci. Technol.*, 2018, 8, 268–275.

12 M. Sahoo, S. Mansingh and K. M. Parida, *J. Mater. Chem. A*, 2019, 7, 7614–7627.

13 X. Ye, Y. Chen, C. Ling, R. Ding, X. Wang, X. Zhang and S. Chen, *Dalton Trans.*, 2018, 47, 10915–10924.

14 S. Zhang, C. Chang, Z. Huang, Y. Ma, W. Gao, J. Li and Y. Qu, *ACS Catal.*, 2015, 5(11), 6481–6488.

15 Q. Xiao, S. Sarina, E. Jaatinen, J. Jia, D. P. Arnold, H. Liuc and H. Zhu, *Green Chem.*, 2014, 16, 4272–4285.

16 D. Han, Z. Bao, H. Xing, Y. Yang, Q. Ren and Z. Zhang, *Nanoscale*, 2017, 9, 6026–6032.

17 D. Sun and Z. Li, *J. Phys. Chem. C*, 2016, 120(35), 19744–19750.

18 D. Sun, M. Xu, Y. Jiang, J. Long and Z. Li, *Small Methods*, 2018, 2(12), 1800164.

19 J. Shen, B. Yan, M. Shi, H. Ma, N. Li and M. Ye, *J. Mater. Chem.*, 2011, 21, 3415–3421.

20 P. Fageria, S. Uppala, R. Nazir, S. Gangopadhyay, C.-H. Chang, M. Basu and S. Pande, *Langmuir*, 2016, 32, 10054–10064.

21 M. Verma, M. B. Newmai and P. S. Kumar, *Dalton Trans.*, 2017, 46, 9664–9677.

22 K. Li, B. Chai, T. Peng, J. Mao and L. Zan, *ACS Catal.*, 2013, 3, 170–177.

23 M. Vippola, M. Valkonen, E. Sarlin, M. Honkanen and H. Huttunen, *Nanoscale Res. Lett.*, 2016, 11, 169.

24 Y. Fu, F. Ning, S. Xu, H. An, M. Shao and M. Wei, *J. Mater. Chem. A*, 2016, 4, 3907–3913.

25 N. Toshima and T. Yonezawa, *New J. Chem.*, 1998, 22, 1179.

26 Y. Mizukoshi, K. Okitsu, Y. Maeda, T. A. Yamamoto, R. Oshima and Y. Nagata, *J. Phys. Chem. B*, 1997, 101, 7033.

27 D. Sahoo, S. Patnaik, D. Rath and K. M. Parida, *Inorg. Chem. Front.*, 2018, 5, 879–896.

28 R. Xie, G. Fan, Q. Ma, L. Yang and F. Li, *J. Mater. Chem. A*, 2014, 2, 7880–7889.

29 M. Sahoo and K. Parida, *ChemistrySelect*, 2018, 3, 3092–3100.

30 K. M. Parida and L. Mohapatra, *Dalton Trans.*, 2012, 41, 1173–1178.

31 Z. Gao, R. Xie, G. Fan, L. Yang and F. Li, *ACS Sustainable Chem. Eng.*, 2017, 5, 5852–5861.

32 S. Singha, M. Sahoo and K. M. Parida, *Dalton Trans.*, 2011, 40, 7130–7132.

33 E. Akhavan and E. Ghaderi, *J. Phys. Chem. B*, 2011, 115, 6279.

34 Y. Yang, H. F. Yao, F. G. Xi and E. Q. Gao, *J. Mol. Catal. A: Chem.*, 2014, 390, 198–205.

35 M. Sahoo, S. Singha and K. M. Parida, *New J. Chem.*, 2011, 35, 2503–2509.

36 R. Nazir, P. Fageria, M. Basu and S. Pande, *J. Phys. Chem. C*, 2017, 121, 19548–19558.

37 H. Gu, Y. Yang, J. Tian and G. Shi, *ACS Appl. Mater. Interfaces*, 2013, 5, 6762–6768.

38 L. Meng, Z. Chen, Z. Ma, S. He, Y. Hou, H.-H. Li, R. Yuan, X.-H. Huang, X. Wang, X. Wang and J. Long, *Energy Environ. Sci.*, 2018, 11, 294–298.

39 J. Zhao, B. Liu, L. Meng, S. He, R. Yuan, Y. Hou, Z. Ding, H. Lin, Z. Zhang, X. Wang and J. Long, *Appl. Catal., B*, 2019, 256, 117823.

40 S. Sarina, H. Zhu, E. Jaatinen, Q. Xiao, H. Liu, J. Jia, C. Chen and J. Zhao, *J. Am. Chem. Soc.*, 2013, **135**, 5793–5801.

41 X. H. Li, M. Baar, S. Blechert and M. Antonietti, *Sci. Rep.*, 2013, **3**, 1743.

42 Z. J. Wang, S. Ghasimi, K. Landfester and K. A. I. Zhang, *Chem. Mater.*, 2015, 27, 1921–1924.

43 T. T. Trinh, R. Sato, M. Sakamoto, Y. Fujiyoshi, M. Haruta, H. Kurata and T. Teranishi, *Nanoscale*, 2015, 7, 12435–12444.

This journal is © The Royal Society of Chemistry 2019